Results in Chemistry 15 (2025) 102237

Contents lists available at ScienceDirect

Results in Chemistry

journal homepage: www.sciencedirect.com/journal/results-in-chemistry

Synthesis, structural characterization, *in vitro* biological evaluation and *in silico* molecular docking of some new 1,2,3-Benzotriazole-based Schiff base derivatives

Shawkat Hayat [a], Mohamed S. Othman [b,c], Hayat Ullah [d,*], Amina Qureshi [a], Fazal Rahim [a,*], Sadiqa Begum [a], Mohsan Nawaz [a], Abdul Wadood [e], Amal H. Al-Bagawi [f], Ahmed M. Aref [c], Mohamed A. Fareid [g], Rashid Iqbal [h,i]

[a] *Depatment of Chemistry, Hazara University, Mansehra 21300, Khyber Pakhtunkhwa, Pakistan*
[b] *Biochemistry Department, College of Medicine, University of Ha'il, Hail 2440, Saudi Arabia*
[c] *Faculty of Biotechnology, October University for Modern Science and Arts (MSA), Giza, Egypt*
[d] *Department of Chemistry, University of Okara, Okara 56130, Pakistan*
[e] *Department of Biochemistry, Abdul Wali Khan University Mardan, Mardan 23200, Pakistan*
[f] *Chemistry Department, Faculty of Science, University of Ha'il, Hail 2440, Saudi Arabia*
[g] *Department of Medical Laboratories, Faculty of Applied Medical Science, University of Ha'il, Hail 2440, Saudi Arabia*
[h] *Department of Agronomy, Faculty of Agriculture and Environment, The Islamia University of Bahawalpur 63100, Pakistan.*
[i] *Department of Life Sciences, Western Caspian University, Baku, Azerbaijan*

ARTICLE INFO

Keywords:
Alpha-glucosidase
Benzotriazole
Molecular docking study
Synthesis
Schiff base
Structure activity relationship

ABSTRACT

1,2,3-benzotriazole-based Schiff base derivatives were synthesized, characterized through different techniques such as ^{1}HNMR, ^{13}CNMR, and HREI-MS, and screened against the alpha-glucosidase enzyme. All the synthesized analogues showed good inhibitory potentials with IC_{50} values ranging from 2.20 ± 0.30 μM to 24.40 ± 0.10 μM as compared to the standard drug acarbose (IC_{50} = 10.30 ± 0.20 μM). The most potent analogues among the series are **3** (IC_{50} = 4.30 ± 0.20 μM), **8** (IC_{50} = 9.40 ± 0.10), **9** (IC_{50} = 6.20 ± 0.40), **10** (IC_{50} = 6.60 ± 0.20), **11** (IC_{50} = 6.10 ± 0.30), **12** (IC_{50} = 4.70 ± 0.50 μM), **13** (IC_{50} = 2.20 ± 0.30 μM), **14** (IC_{50} = 4.30 ± 0.20 μM), and **16** (IC_{50} = 7.40 ± 0.20), which were found manyfold more active than the standard drug acarbose. A structure-activity relationship study was established that significantly depends on the position, nature, number, and electron-donating/withdrawing effect of the substituent(s) attached to the phenyl ring. We conducted molecular docking studies to investigate the binding interaction of the most potent analogues with the active site of an enzyme.

1. Introduction

Diabetes mellitus (DM) is a metabolic condition defined by chronically high blood sugar levels [1]. The International Diabetes Federation Diabetes Atlas estimates that it affected 537 million people globally in 2021, and that number is expected to rise to 643 million by 2030 [2]. Diabetes mellitus was the ninth major cause of mortality in a worldwide study conducted by the World Health Organization (WHO) (2019), and it is projected to be the seventh leading cause of death by 2030 [3]. Pancreatic cells generate the insulin hormone, which plays a crucial role in regulating blood glucose levels. It is required for several cellular activities such as glucose absorption and transport, glycogen synthesis, protein synthesis, and fatty acid synthesis. Inadequate insulin production or insulin resistance hinders proper glucose homeostasis, resulting in hyperglycemia [4]. Chronic hyperglycemia can have major long-term consequences such as cardiovascular disease, nerve damage, and renal failure [5]. Depending on the mechanism of its manifestation, diabetes mellitus can be categorized into three types: type 1 diabetes mellitus (T1DM), type 2 diabetes mellitus (T2DM), and gestational diabetes. T1DM affects roughly 5–10 % of all diabetes patients and is characterized by the death of pancreatic insulin-producing β-cells destroyed by the immune system, resulting in an extreme shortage of insulin, hyperglycemia, inflammation, oxidative damage, and other metabolic problems [6,7]. Over 90 % of people worldwide suffer from T2DM, with a

* Corresponding authors.
E-mail addresses: ayaanwazir366@gmail.com (H. Ullah), fazalstar@gmail.com (F. Rahim).

https://doi.org/10.1016/j.rechem.2025.102237
Received 14 December 2024; Accepted 1 April 2025
Available online 9 April 2025

projected increase to 592 million by 2035 [8]. T2DM is characterized by insulin resistance resulting from insulin receptor insensitivity, persistent hyperglycemia, dyslipidaemia, and low-level inflammation [9]. Gestational diabetes occurs only during pregnancy in women and results in unfavourable clinical conditions in both the mother and her kids [10]. Hyperglycemia is the most serious criterion of all forms of diabetes, and it can lead to a variety of complications such as cardiovascular disease, neuropathy, renal failure, lipid metabolism issues, and many others. Therefore, controlling blood glucose levels in diabetes individuals is very critical [11,12]. Reduced postprandial hyperglycemia is one treatment method for treating diabetes in its early stages. This is accomplished by suppressing the carbohydrate-hydrolysing enzymes, α-glucosidase and α-amylase, in the digestive system, which prevents glucose absorption. So, drugs that block these enzymes make it take longer for glucose to be absorbed, which lowers the rise in plasma glucose after a meal [13,14]. Since the 1990s, anti-diabetic medicines with *α*-glucosidase inhibitory capabilities, such as acarbose, miglitol, and voglibose, have been commercially accessible for treating postprandial hyperglycemia [15].

Heterocyclic compounds containing a fused benzene ring and an azole ring are called benzo-fused azoles [16,17]. The azole ring typically contains one or more nitrogen atoms. Benzotriazole is a benzo-fused azole containing three nitrogen atoms [18]. Benzotriazole and its derivatives show a variety of biological activities, including antifungal and antibacterial [19,20], anti-proliferative [21], anti-cancer [22], and antidiabetic [23]. In medicinal chemistry, benzotriazoles showed an extensive range of applications, as demonstrated by drugs such as Alizapride and Varazole (Fig. 1) [24,25].

Schiff base is a nitrogen analogue of an aldehyde or ketone in which the carbonyl group is condensed with a primary amine [26]. These compounds occur naturally as well as synthesized in the laboratory and have great significance in chemistry and biochemistry [27]. They have a variety of applications in analytical, inorganic, and organic chemistry. For example, they are used as catalysts, dyes, luminescence chemosensors, and for solar energy applications as well [28]. The biological activities of Schiff bases include antibacterial [29], antifungal [30], anticancer [31], anti-urease [32], antiviral [33], and anti-Alzheimer's [34] activities.

In the past, researchers had synthesized triazole [35–37] and Schiff base analogues [38,39] as α-glucosidase and α-amylase inhibitors (Fig. 2). In the present work, a new series of benzotriazole-based Schiff base analogues **(1–18)** has been synthesized successfully and evaluated for their *α*-glucosidase inhibitory activity. The result obtained about their biological potential was found to be better on the basis of IC_{50} values than the earlier work and provides a basis for further investigation in future research work.

2. Results and discussion

2.1. Chemistry

Benzotriazole (**I,** 3 mmol) was mixed with ethyl 2-bromoacetate (3 mmol) in acetone (15 mL) in the presence of K_2CO_3, and the reaction mixture was stirred under reflux conditions to yield methyl 2-(1*H*-benzo[d][1,2,3]triazol-1-yl)acetate as the first intermediate product (**II**). The intermediate product (**II,** 1 mmol) was further reacted and refluxed with hydrazine hydrate (10 mL) in MeOH (10 mL) to afford 2-(1*H*-benz-[d][1, 2, 3]triazol-1-yl) acetohydrazide as the second intermediate product (**III**). The intermediate product (**III,** 0.5 mmol) was further treated with substituted benzaldehydes (0.5 mmol) in methanol (15 mL) to obtain benzotriazole-based Schiff base derivatives (**1–18**) (Scheme 1, Table 1). Thin layer chromatography (TLC) initially confirmed each and every step. We washed the final product with *n*-hexane to obtain pure products. For further characterization of the compounds, spectroscopic techniques including ^{1}H NMR, ^{13}C NMR and HREI-MS were used.

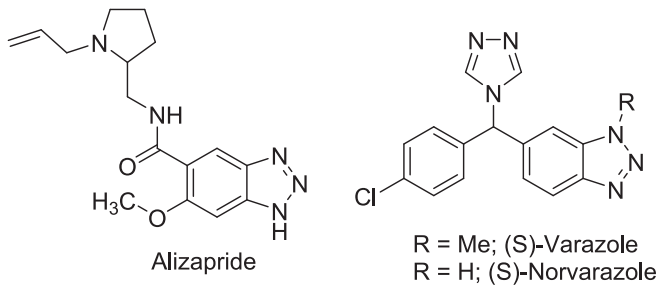

Fig. 1. Structure of benzotriazoles containing moieties.

2.2. In vitro alpha glucosidase inhibitory activity

All the synthesized analogues were tested for their alpha-glucosidase inhibitory potential and found them active and showed excellent inhibitory activity with IC_{50} values ranging from 2.20 ± 0.30 μM to 24.40 ± 0.10 μM as compared to the standard drug acarbose (IC_{50} = 10.30 ± 0.20 μM) (Table 2).

2.2.1. Structure-activity relationship

A structure-activity relationship study was established that significantly depends on the position, nature, number, and electron-donating/withdrawing effect of the substituent(s) attached to one of the phenyl rings. The basic skeleton of benzotriazole analogues is the same, but they differ from each other *via* substitution on one of the phenyl rings.

Hydroxyl-substituted analogues have maximum potential among the whole series, and this may be due to the hydroxyl group being involved in hydrogen bonding, making the analogues more favourable for enzyme inhibition due to better interaction with the active site of the enzyme. If we compare analogue **13** (IC_{50} = 2.20 ± 0.30 μM) having 4-hydroxy substitution with analogues **15** (IC_{50} = 4.30 ± 0.60 μM) having 3-hydroxy substitution and **16** (IC_{50} = 7.40 ± 0.20 μM) having 2-hydroxy substitution. These derivatives have the same substituents, but there is a slight difference in the activity of these analogues. This is because of the relative position of the hydroxyl group on the phenyl ring. The hydrogen bonding effect of the hydroxyl group activates the ring and makes it more active and favourable for enzyme inhibition.

The analogue **3** (IC_{50} = 4.30 ± 0.20 μM) having 2-fluoro substitution has excellent inhibitory potential because of its highly electron-withdrawing nature, small size, and involvement in hydrogen bonding toward the active site of the enzyme. The presence of hydrogen bonding, the strong electron-withdrawing nature, and the small size of the fluoro group may enhance the inhibitory potential, making it more favourable to interact with the active site of the enzyme.

The inhibitory potential of the analogues **10** (IC_{50} = 6.60 ± 0.20 μM) having 2-nitro substitution, **11** (IC_{50} = 6.10 ± 0.30 μM) having 3-nitro substitution, and **12** (IC_{50} = 4.70 ± 0.50 μM) having 4-nitro substitution were compared. These analogues have the same substituents, but there is a slight difference in the activity of these analogues. This is because of the relative position of the nitro group on the phenyl ring. The involvement of the nitro group in hydrogen bonding and its electron-withdrawing nature may activate the ring and make it more active and favourable for enzyme inhibition. Analogue **10** (having 2-nitro substitution) is less potent compared to the analogues having para and *meta* substitution. The high potency of analogue **12** indicated that nitro groups at *para* positions are more favourable for inhibition.

The activity of analogue **8** (IC_{50} = 9.40 ± 0.10 μM) having 2-chloro substitution and analogue **9** (IC_{50} = 6.20 ± 0.40 μM) having 4-chloro substitution were compared. There is a slight difference in the inhibitory potential of these analogues, and this difference may be due to the different position of the chloro group on the phenyl ring. The activating effect of the chloro group is enhanced at the para position compared to *the ortho* position, making analogue **9** more potent than analogue **8**.

By comparing analogues **4** (IC_{50} = 11.60 ± 0.20 μM) having 4-

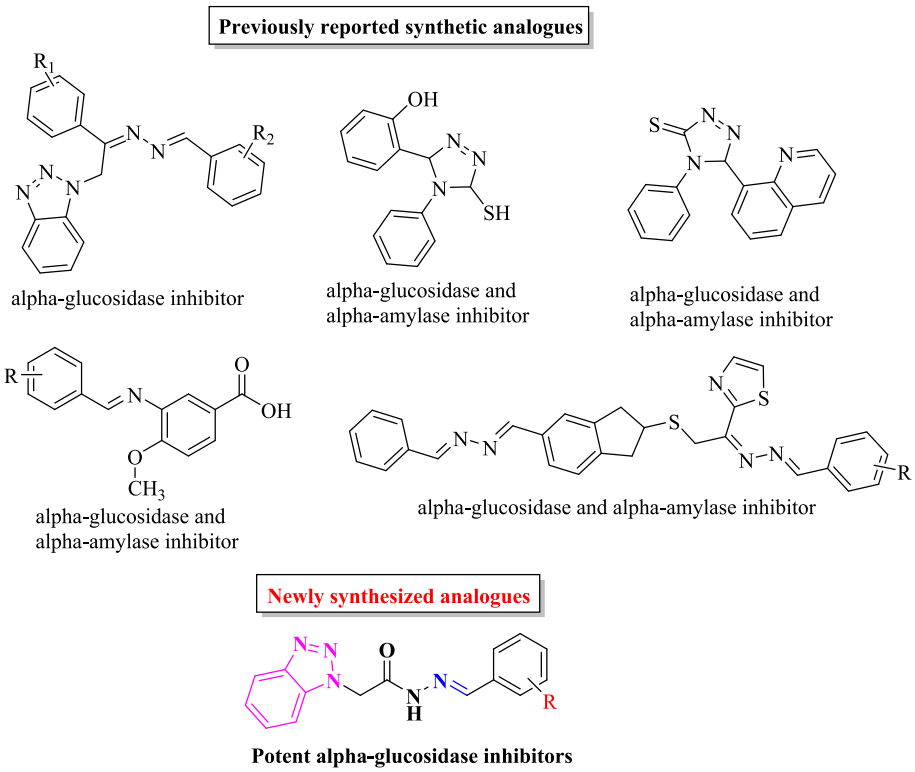

Fig. 2. Rationalization of the current work.

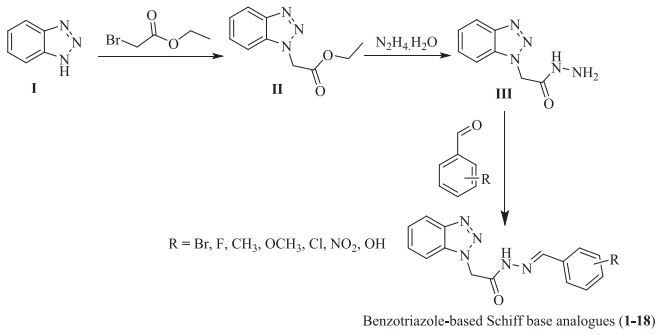

Scheme 1. Synthesis of benzotriazole-based Schiff base analogues.

methyl substitution, **5** (IC_{50} = 13.10 ± 0.60 μM) having 3-methyl substitution, and **6** (IC_{50} = 11.90 ± 0.10 μM) having 2-methyl substitution, a little bit of difference is observed in their activity because of the relative position of the methyl group on the phenyl ring.

The analogues **17** (IC_{50} = 11.70 ± 0.50 μM) having 3-methoxy substitution and **18** (IC_{50} = 15.10 ± 0.40 μM) having 2-methoxy substitution were compared. Analogue **17** is more potent than analogue **18,** and the higher activity indicates that methoxy groups at the 4-position are more favourable for inhibition.

The activity of analogues **1** (IC_{50} = 24.40 ± 0.10 μM) having 3-bromo substitution and **2** (IC_{50} = 19.30 ± 0.30 μM) having 2-bromo substitution were compared. The difference in the activity of these analogues is due to the relative position of the same substituent. Moreover, these analogues have minimum potential among the series because of the relatively bulky size of bromine that may cause steric hindrance toward the enzyme active site, making it a less potent inhibitor.

2.3. Molecular docking study

To investigate the binding interactions between the synthesized compounds and the target enzyme, alpha-glucosidase, a molecular docking study was performed using docking software AutoDock Vina and Pymol. The crystal structure of alpha-glucosidase (PDB ID: 3w37) was retrieved from the Protein Data Bank. The protein structure was prepared by removing water molecules, adding hydrogen atoms, and assigning partial charges. The synthesized compounds were prepared by optimizing their structures using molecular modeling software, Chemdraw. The docking protocol was set up using [docking software]. The binding site was defined as a sphere with a radius of 12 Å centered on the active site of the enzyme. 4. Docking Analysis: The docking results were analyzed by evaluating the binding affinity (ΔG) and the binding mode of each compound. The molecular docking study revealed that the synthesized compounds exhibit high binding affinity toward alpha-glucosidase. The molecular docking study provides valuable insights into the binding interactions between the synthesized compounds and alpha-glucosidase. The results suggest that the compounds exhibit high binding affinity and specificity toward the target enzyme, which is consistent with the biological activity results. The molecular docking (MD) approach is widely used for *in silico* analysis of the biomolecular interactions and binding properties of the synthesized compounds (**1–18**) with the corresponding target protein α-glucosidase. The docking results of the synthesized compounds with the α-glucosidase enzyme provided valuable information regarding the nature of the binding mode, which was highly associated with the experimental results. The MD analysis demonstrates that the docked conformations of almost all of the synthesized compounds are appropriately orientated toward the catalytic residues, making sufficient interactions with the active-site residues of the target enzyme. The structural representation of the targeted enzyme with the docked compounds to the active site was depicted in (Fig. 3 **A).**

Typically, the binding mode analysis revealed that the resulting scaffold possesses both electron-withdrawing groups (EWGs) and electron-donating groups (EDGs) at ortho/para and meta positions.

Consequently, the most potent scaffold in the current series, **13 and 15,** exhibited the same hydroxyl (OH) group at ortho/para position.

Table 1
Different structures of benzotriazole-based Schiff base analogues.

S. No	Structure	S. No	Structure
1	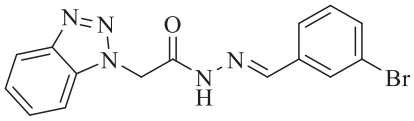	10	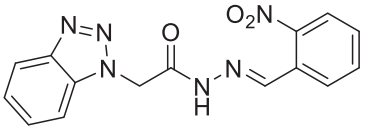
2	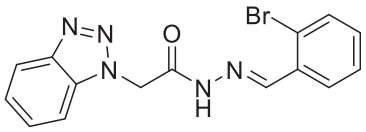	11	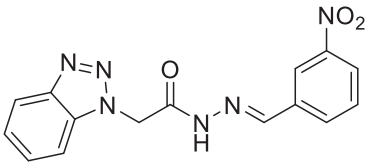
3	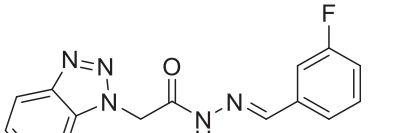	12	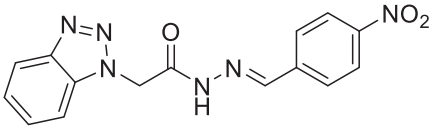
4	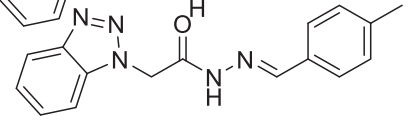	13	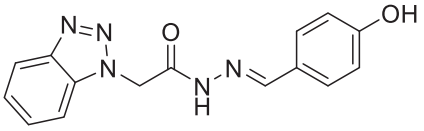
5	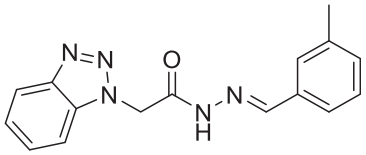	14	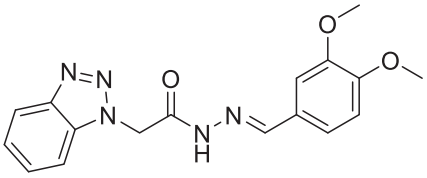
6	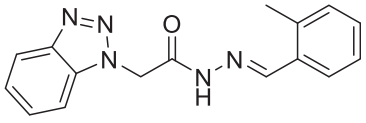	15	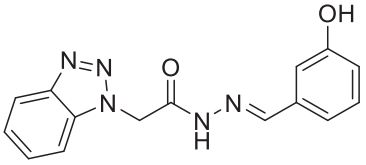
7	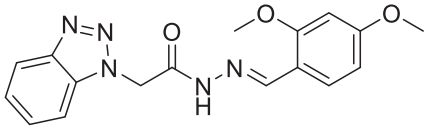	16	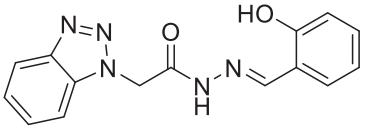
8	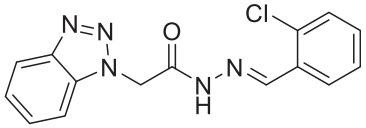	17	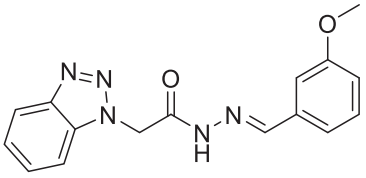
9	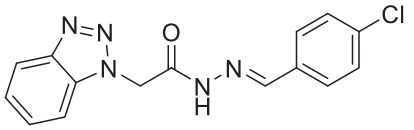	18	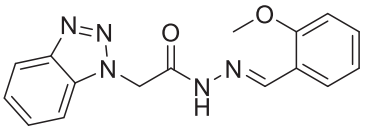

Compound **13** features an OH group positioned ortho to the benzene ring, while compound **15** places the OH group at the para position. Through computational docking studies, analogue **13** exhibited a notably higher docking score and IC_{50} value **(DS: -5.8096, $IC_{50} = 2.20 \pm 0.30$)** compared to **15 (DS: -6.6539, $IC_{50} = 4.30 \pm 0.60$)**, indicating stronger binding affinity to the active site of alpha-glucosidase. The ortho position of the OH group in analogue **13** places it closer to the core of the molecule compared to the para position in analogue **15**.

This closeness might make it easier for key residues in the enzyme's active site to interact with each other in the best way, which would improve the inhibitory activity. Therefore, analogue **13** formed strong hydrogen bond donor interaction with key residue ASP 214 and hydrogen bond donor and hydrogen bond acceptor interaction with ASN 347, while pi-pi interaction with PHE 300; similarly, analogue **15** shows

Table 2
Alpha-glucosidase inhibitory activity of benzotriazole-based Schiff base analogues.

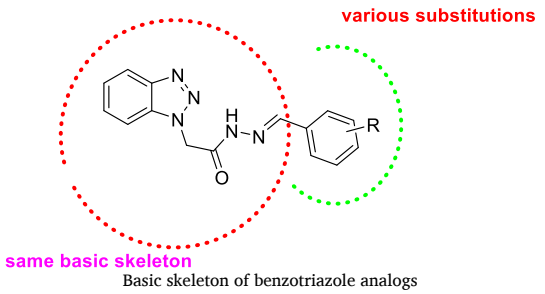

Basic skeleton of benzotriazole analogs

S. NO	IC_{50} (μM) α-glucosidase	S. NO	IC_{50} (μM) α-glucosidase
1	24.40 ± 0.10	10	6.60 ± 0.20
2	19.30 ± 0.30	11	6.10 ± 0.30
3	4.30 ± 0.20	12	4.70 ± 0.50
4	11.60 ± 0.20	13	2.20 ± 0.30
5	13.10 ± 0.60	14	13.30 ± 0.10
6	11.90 ± 0.10	15	4.30 ± 0.60
7	17.30 ± 0.50	16	7.40 ± 0.20
8	9.40 ± 0.10	17	11.70 ± 0.50
9	6.20 ± 0.40	18	15.10 ± 0.40
Acarbose	**10.30 ± 0.20 μM**	**Acarbose**	**10.30 ± 0.20 μM**

strong hydrogen acceptor interaction with ARG 312 and hydrogen donor interaction with ASP 408, while pi-H interaction with ASP 349, as shown in (Fig. 3B, C**).** These findings underscore the importance of molecular positioning in optimizing the inhibitory activity of compounds targeting alpha-glucosidase, providing valuable insights for further drug development efforts in managing diseases such as diabetes mellitus.

Similarly, in this study we evaluated another potent scaffold **(3 and 12),** which show active inhibitory potential containing fluoride (F) and nitro (NO_2) functional groups at *ortho/para* positions on a benzene ring. The compounds' ability to bind and stop other molecules from working was greatly affected by these electron-withdrawing groups. Thus, the result of docking simulations revealed that compounds **3** and **12** also exhibited high docking scores and IC_{50} values **(DS: -6.5884, IC_{50}: 4.30 ± 0.20)** and **(DS: -6.6533, IC_{50}: 4.70 ± 0.50).** The compounds also shared some typical PLI profile, *i.e.*, compound **3** and **12** both show strong H-donor interactions with the same side chain residues, ASP 408, and pi-pi interaction with PHE 300, while different interactions with some key residues, such as compound **3,** formed strong H-acceptor interactions with ASN 347, and compound **12** formed H-donor interactions with ASP 349 within the enzyme's binding pocket as shown in (Fig. 3D, E**).** Thus, the result demonstrated that the electron-withdrawing properties of the nitro and fluoride groups create a more favourable electronic environment for binding, enhancing the inhibitory efficacy. The nitro group increases the electron deficiency of the benzene ring, facilitating strong hydrogen bonding and electrostatic interactions, while the fluoride group further polarizes the environment, promoting binding stabilization. The docked view of the least active compound **1** depicts that the resulting compound at *meta* position does not enter deep into the active site cavity; however, it resides at the entrance loop and only interacts with the side chains of PHE300 and ARG312 (Fig. 3F**),** showing the least inhibition as compared to the rest of the compounds. Thus, the overall description of the MD study shows that the high potency of the compounds against *the* α-glucosidase enzyme may be due to variations in EWGs and EDGs at *ortho/para* directing positions, as well as strong hydrogen bond interactions with side chain residues in the binding pocket, which resulted in stable activity and may enhance enzymatic potency. Interaction details for all synthesized analogues against α-glucosidase enzyme are given in Table 3. To validate the docking results, we performed a redocking procedure to reassess the binding of the synthetic compounds to the alpha-glucosidase enzyme's active site. The results of the redocking procedure were consistent with our previous findings, with only slight modifications. For instance, the most active compound in the series, analogue **13**, again demonstrated higher binding affinity and tightly bound to the same position in the enzyme's active site, confirming the accuracy of our initial docking results. The redocking results reaffirmed that these compounds fit well

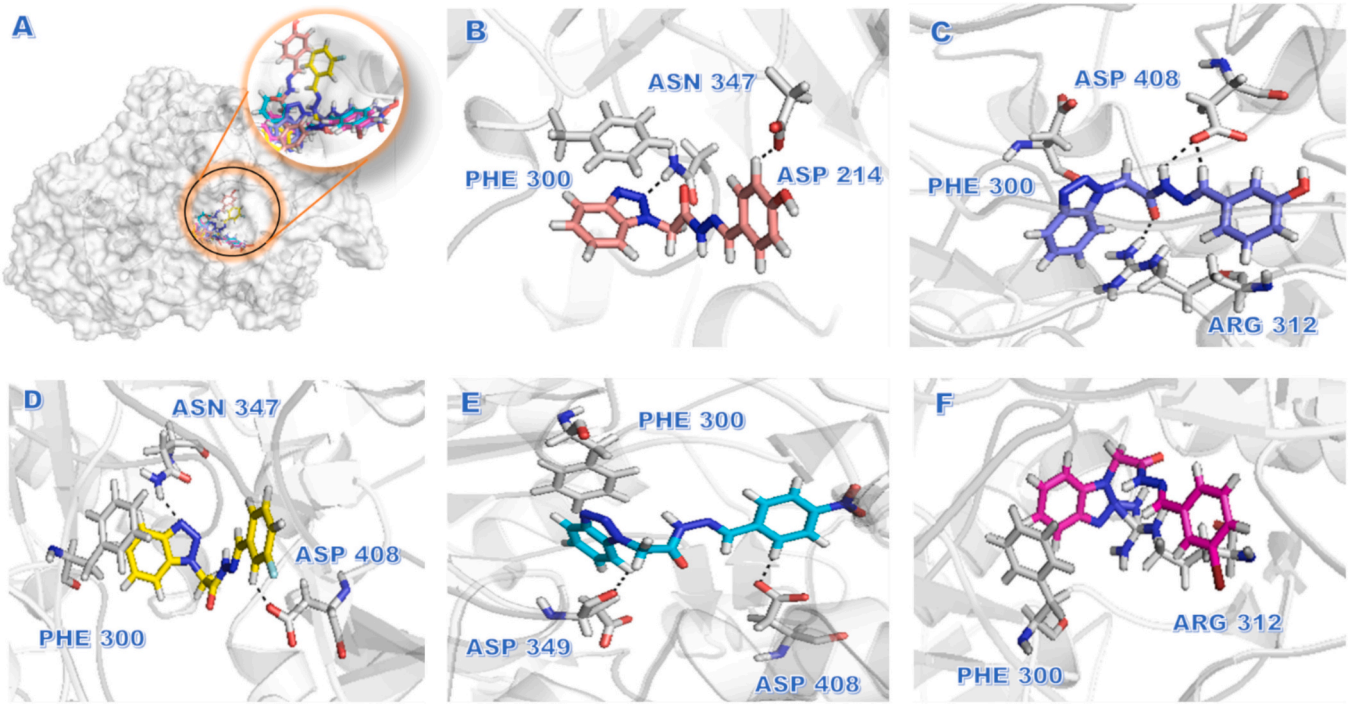

Fig. 3. Protein–ligand interaction (PLI) profile of the synthesized compounds (**1–18**) against α-glucosidase enzyme. Fig. (1 A) indicates the surface representation of the α-glucosidase enzyme. Fig. (1B—1F) Indicates PLI profile for the tested active compound (**13B**), (**15C**), (**3D**), (**12E**), and (**1F**). Double-sided arrows represent the arene–arene interaction.

Table 3
Interaction details for synthesized compounds against α-glucosidase enzyme.

S. No	Interaction		Details			Docking Score
	Ligand	Receptor	Interaction	Distance	E kcal/mol	
1	6-ring	N ARG 312	pi-H	4.35	−1.1	−6.9259
	6-ring	6-ring PHE 300	pi-pi	3.70	−0.0	
2	6-ring	N ARG 312	pi-H	4.36	−0.8	−6.7772
	6-ring	6-ring PHE 300	pi-pi	3.72	−0.0	
3	C 32	OD2 ASP 408	H-donor	2.83	−0.9	−6.5884
	N 3		H-acceptor	3.06	−2.2	
	6-ring	ND2 ASN 347	pi-pi	3.77	−0.0	
		6-ring PHE 300				
4	6-ring	N ARG 312	pi-H	4.39	−0.5	−6.8099
	6-ring	6-ring PHE 300	pi-pi	3.88	−0.0	
5	C 14	O VAL 303	H-donor	3.39	−1.0	−5.8836
	5-ring	6-ring PHE 300	pi-pi	3.42	−0.0	
	6-ring		pi-pi	3.63	−0.0	
		6-ring PHE 300				
6	N 19	OD2 ASP 408	H-donor	3.21	−1.1	−6.9696
	O 18		H-acceptor	3.13	−1.2	
	6-ring	NE ARG 312	pi-pi	4.48	−1.1	
		N ARG 312				
7	N 2	NH1 ARG 439	H-acceptor	3.58	−1.7	−7.1791
8	6-ring	N ARG 312	pi-H	4.39	−0.7	−6.6924
	6-ring	6-ring PHE 300	pi-pi	3.69	−0.0	
9	C 14	OD1 ASN 347	H-donor	3.23	−1.6	−6.2914
	6-ring		pi-pi	3.40	−0.0	
		6-ring PHE 300				
10	C 14	OD1 ASP 214	H-donor	2.49	−0.7	−6.9992
	N 2		H-acceptor	3.63	−0.7	
	6-ring	NH2 ARG 212	Pi-cation	4.11	−0.0	
		NH1 ARG 439				
11	C 25	OD2 ASP 408	H-donor	3.02	−1.1	−7.0395
	O 36		H-acceptor	3.33	−0.6	
	6-ring	NE2 HIS 111	Pi-pi	2.73	−0.0	
		6-ring PHE 300				
12	C 14	O ASP 349	H-donor	3.12	−1.4	−6.6533
	C 32	OD2 ASP 408	H-donor	3.28	−0.8	
	6-ring		Pi-pi	3.89	−0.0	
	6-ring	6-ring PHE 300	Pi-pi	3.99	−0.0	
		6-ring PHE 300				
13	C 14	OD1 ASN 347	H-donor	3.53	−0.5	−5.8096
	C 27		H-donor	2.86	−0.6	
	N 2	OD2 ASP 214	H-acceptor	2.58	−0.9	
	5-ring		Pi-pi	3.96	−0.0	
		ND2 ASN 347				
		6-ring PHE 300				
14	O 18	NH2 ARG 312	H-acceptor	2.63	−0.8	−7.8316
	5-ring		Pi-pi	3.01	−0.0	
		6-ring PHE 300				
15	N 19	OD2 ASP 408	H-donor	3.04	−1.9	−6.6539
	C 22		H-donor	2.75	−1.3	
	O 18	OD2 ASP 408	H-acceptor	2.71	−2.6	
	5-ring		Pi-pi	4.30	−0.8	
		NE ARG 312				
		CB ASP 349				
16	5-ring	6-ring PHE 300	Pi-pi	3.24	−0.0	−6.5700
17	C 27	O VAL 303	H-donor	2.84	−0.5	−6.6793
	O 18	CD ARG 439	H-acceptor	2.88	−0.5	
	5-ring	CD ARG 312	Pi-pi	4.15	−0.6	
18	O 34	NH1 ARG 439	H-acceptor	2.93	−1.5	−7.1999
	5-ring		Pi-pi	3.23	−0.0	
		6-ring PHE 300				

into the enzyme's binding site, forming strong interactions with key residues, which is consistent with their experimental inhibitory activity. In contrast, the least active compound, analogue 1, failed to penetrate deeply into the active site and showed weaker binding energy and minimal interactions, which aligns with its lower IC_{50} value. This redocking validation, consistent with both the initial docking results and experimental data, provides further confidence in the accuracy and reliability of our molecular docking predictions.

2.4. Density functional theory (DFT)

To get insights in to the electronic properties of derivatives, density functional theory (DFT) analysis was performed. All DFT calculations for compounds 3, 13 and 15 were carried out using the Gaussian 09 quantum package [40]. Geometrical optimization of active analogues was conducted at wb97XD/6-31 g(d,p) level [41,42]. The wb97XD functional was employed to validate the altered structure and accuracy of results, as well as to investigate electronic parameters. Furthermore, vibrational frequency analysis was conducted to confirm the minimum energy structures through potential energy surface (PES) phenomena. FMO was carried out to determine the electronic properties of the compounds, while molecular electrostatic potential (MESP) was to locate the reactive sites responsible for binding interactions with targeted enzymes. The Gauss View (5.0) and ChemCraft software were utilized to visualize the molecular geometry and electronic density [43].

2.4.1. Molecular electrostatic potential (MESP)

To understand the physiochemical features of the potent analogues, molecular electrostatic potential (MESP) was employed. MESP is a valuable tool for predicting various physiochemical properties, including charge distribution, electronic structure and reactivity. The MESP maps provide a visual representation of the electrostatic potential in overall molecules [44–46], which is used to identify regions susceptible to nucleophillic or electrophilic attacks. The positive regions, indicated through blue color, represents region where nucleophillic attacks are likely to occur, while the negative regions, represented through red color, indicates region which is more susceptible to electrophilic attacks. These different colors are assigned to different regions on the MESP map, provide valuable insights into the electronic properties of the compounds. Mostly nitrogen containing moieties have negative potential like triaozle ring, due to lone pair of nitrogen atoms as they were involved in making interactions with electrophilic moiety of targeted amino acids. Similarly, for analog 13 and 15 oxygen atom act as nucleophillic site while hydrogen attached t oxygen atom in hydroxyl group is highly electrophilic point, which get attacked by nucleophilic moiety from targeted amino acids. All these results were depicted in **(Figs. 4–6).**

2.4.2. Frontier molecular orbital (FMO) theory

To investigate the chemical reactivity of potent molecules in the synthesized compounds, FMO analysis was performed. Specifically molecular orbitals (HOMO and LUMO) were examined [47]. The HOMO-LUMO energy gap for analog 3, 13 and 15 provide valuable

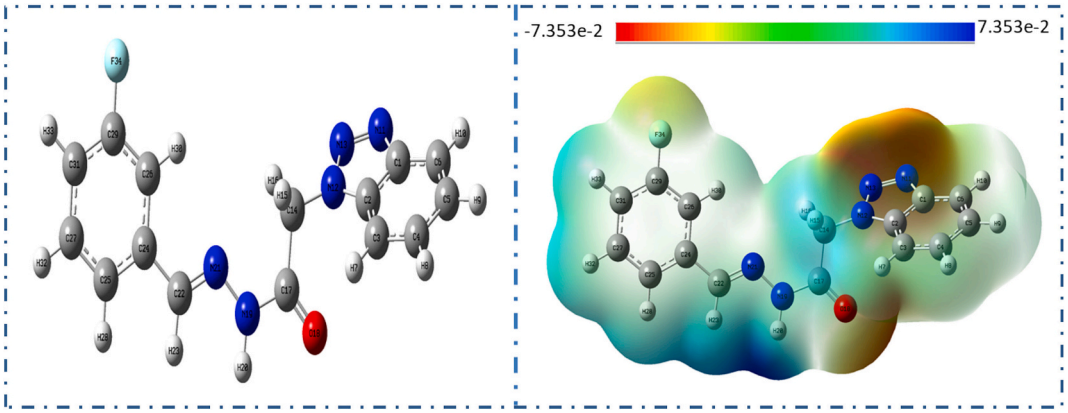

Fig. 4. Represents electron density and electrostatic potential of analog 3.

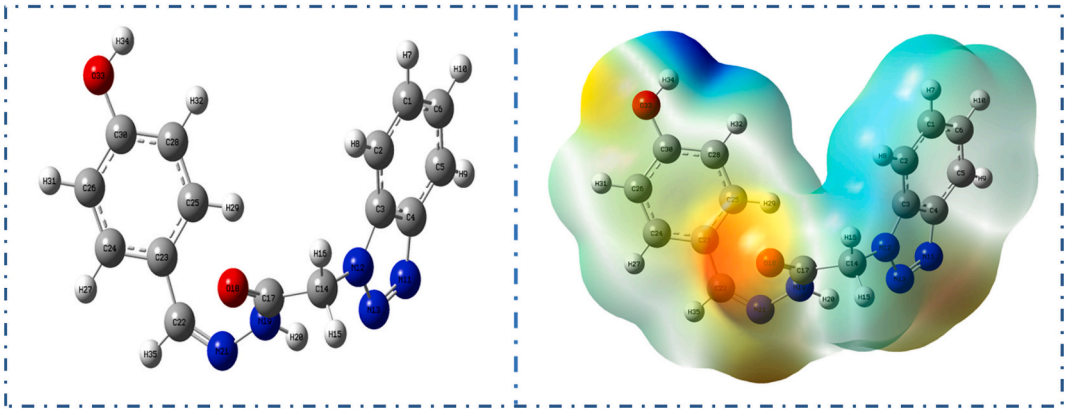

Fig. 5. Represents electron density and electrostatic potential of analog 13.

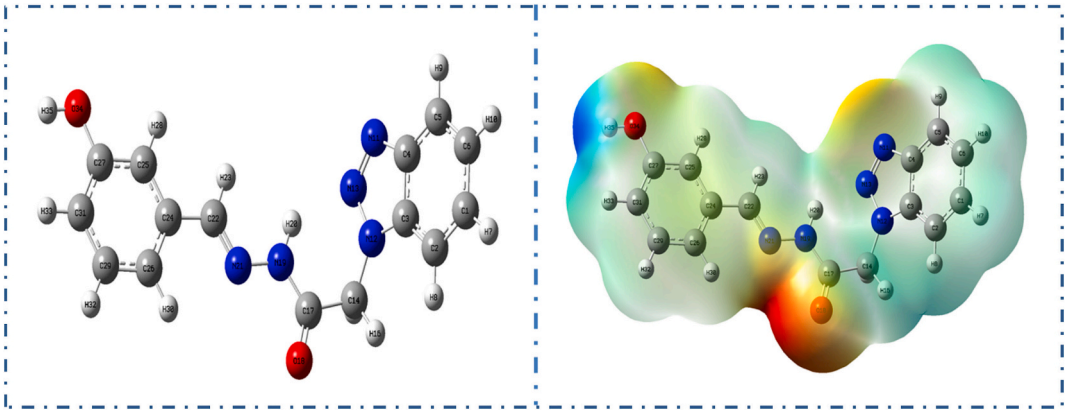

Fig. 6. Represents electron density and electrostatic potential of analog 15.

insights in to their stability and reactivity. A smaller energy gap indicates higher reactivity. The distribution and energy values of HOMO and LUMO orbitals also revealed electron donating and accepting capabilities. For all these analogues 3, 13 and 15 HOMO orbital contain lobes on substituted phenyl ring while for LUMO orbital lobes formed on benzotriazole moiety. This different arrangement of electronic density and lobe formation is due to different attached functional groups and shifting of these electronic densities from higher to lower regions. All these results for FMO analysis were illustrated in (Figs. 7–9) to understand relative stability and reactivity of molecules.

3. Material and methods

We purchased all chemicals and solvents from Sigma Aldrich, ensuring their purity ranged from 97 to 99 %. We recorded NMR spectra on a Bruker Advance AM spectrometer, using DMSO as the solvent. We measured the chemical shifts in relation to TMS as an internal standard. We ran the high-resolution mass spectra (electron impact, 60 eV) on a Finnigan MAT-311 A instrument (Germany). For visualization of the chromatogram, a UV lamp (Schimazdu, Germany) of wavelength 254/365 was used.

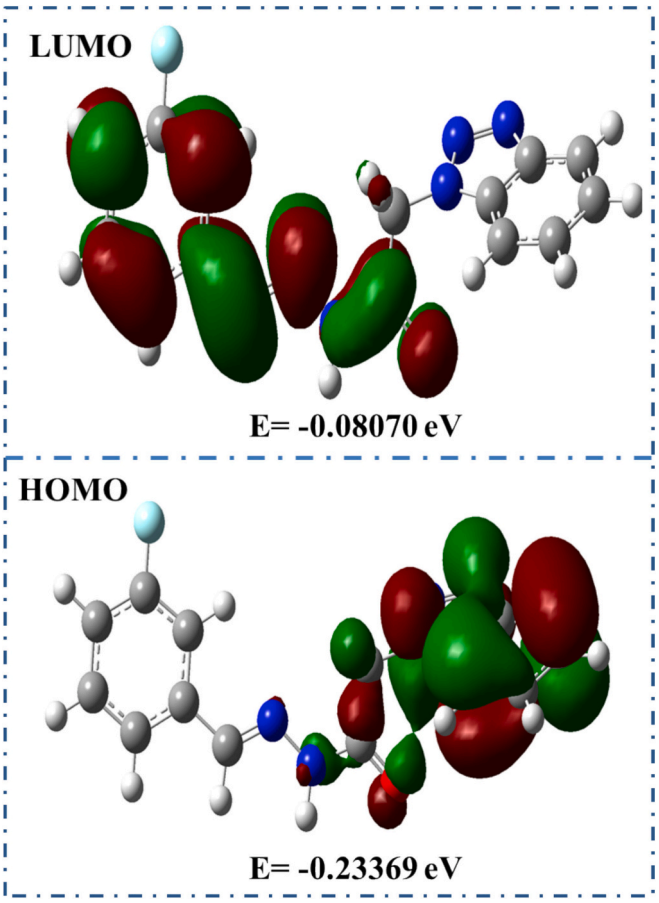

Fig. 7. FMO outcomes and HOMO-LUMO energy gap of analogue **3.**

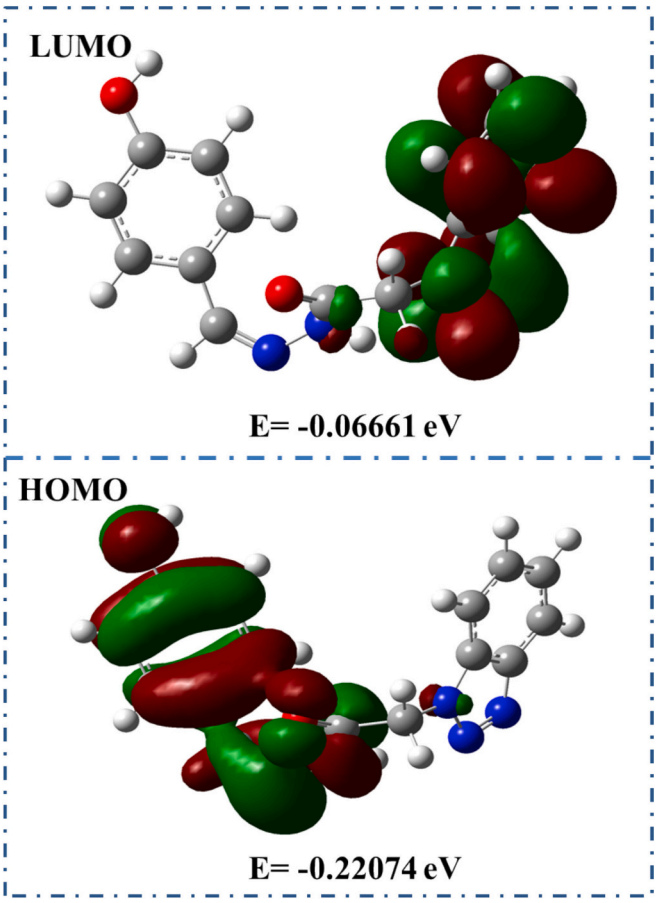

Fig. 8. FMO outcomes and HOMO-LUMO energy gap of analog 13.

3.1. General procedure for the synthesis of Benzotriazole based Schiff base derivatives

Benzotriazole was mixed with ethyl 2-bromoacetate in acetone in the presence of K_2CO_3, and the reaction mixture was stirred under reflux conditions to yield methyl 2-(1*H*-benzo[d][1, 2, 3]triazol-1-yl)acetate as intermediate product (I), which was further reacted and refluxed with an equimolar amount of hydrazine hydrate in MeOH to afford 2-(1*H*-benz-[d][1, 2, 3]triazol-1-yl) acetohydrazide as intermediate product (**II**). The intermediate product (**II**) was further treated with substituted aldehydes to obtain benzotriazole-based Schiff base derivatives.

3.2. Spectral analysis

3.2.1. 2-(1H-benzo[d][1,2,3]triazol-1-yl)-N′-(3-bromobenzylidene) acetohydrazide

^{1}H NMR (500 MHz, DMSO-d_6): the peak at δ 11.63 is singlet and represent the NH proton, the peak at 8.43 represent the singlet which is for imine N═CH which confirm the reaction completion, Similarly other proton related to Triazole or phenyl ring of benzaldehyde appear at various chemical shift value ranging from 8.17 to 7.41 ppm, such as at 8.17 (d, J = 7.8 Hz, 1H, ArH), 7.91 (d, J = 7.4 Hz, 1H, ArH), 7.81 (s, 1H, ArH), 7.63 (t, J = 7.5 Hz, 1H, ArH), 7.62 (d, J = 7.1 Hz, 1H, ArH), 7.54 (d, J = 7.1 Hz, 1H, ArH), 7.41 (m, 1H, ArH), 7.38 (t, J = 7.5 Hz, 1H, ArH). The peak at 5.53 is for CH_2 which confirm the presence of both Triazole and phenyl ring of benzaldehyde in the final product.

^{13}C NMR (125 MHz, DMSO-d_6): δ the proton decouple spectra were taken for carbon 13 for all product which show various singlet peak for various carbons at 168.5 (C), 143.2 (CH), 141.2 (C), 133.4 (C), 131.6 (C), 131.1 (CH), 130.8 (CH), 129.4 (CH), 126.6 (CH), 123.3 (CH), 123.1 (CH), 122.5 (C), 121.2 (CH), 113.3 (CH), 61.4 (CH_2), HREI-MS: *m/z* calcd for $C_{15}H_{12}BrN_5O$ $[M]^+$ 357.0225; Found: 357.0210.

3.2.2. 2-(1H-benzo[d][1,2,3]triazol-1-yl)-N′-(2-bromobenzylidene) acetohydrazide

^{1}H NMR (500 MHz, DMSOd_6) δ 11.58 (s, 1H, NH), 8.32 (s, 1H, N═CH), 8.11 (d, J = 7.8 Hz, 1H, ArH), 7.93 (d, J = 7.4 Hz, 1H, ArH), 7.65 (d, J = 7.2 Hz, 1H, ArH), 7.66 (t, J = 7.6 Hz, 1H, ArH), 7.51 (d, J = 7.2 Hz, 1H, ArH), 7.41 (t, J = 7.1 Hz, 1H, ArH), 7.37 (m, 1H, ArH), 7.32 (t, J = 7.5 Hz, 1H, ArH), 5.49 (s, 2H, CH_2), ^{13}C NMR (125 MHz, DMSOd_6) δ 168.3 (C), 141.9 (CH), 141.7 (C), 134.4 (C), 131.7 (C), 130.6 (CH), 130.2 (CH), 126.8 (CH), 126.5 (CH), 122.5 (CH), 122.6 (CH), 119.9 (C), 119.4 (CH), 112.8 (CH), 61.1 (CH_2), HREI-MS: *m/z* calcd for $C_{15}H_{12}BrN_5O$ $[M]^+$ 357.0225; Found; 357.0210.

3.2.3. 2-(1H-benzo[d][1,2,3]triazol-1-yl)-N′-(3-fluorobenzylidene) acetohydrazide

^{1}H NMR (500 MHz, DMSOd_6) δ 11.71 (s, 1H, NH), 8.48 (s, 1H, N═CH), 8.26 (d, J = 7.8 Hz, 1H, ArH), 7.97 (d, J = 7.4 Hz, 1H, ArH), 7.87 (s, 1H, ArH), 7.69 (t, J = 7.5 Hz, 1H, ArH), 7.65 (m, 1H, ArH), 7.58 (dd J = 7.2, 1.9 Hz, 1H, ArH), 7.47 (dd J = 7.1, 1.9 Hz, 1H, ArH), 7.44 (t, J = 7.6 Hz, 1H, ArH), 5.58 (s, 2H, CH_2), ^{13}C NMR (125 MHz, DMSOd_6) δ 170.3 (C), 161.2 (C), 147.9 (CH), 145.1 (C), 136.4 (C), 132.3 (C), 131.1 (CH), 125.9 (CH), 125.4 (CH), 124.2 (CH), 121.4 (CH), 118.7 (CH), 117.5 (CH), 114.6 (CH), 63.3 (CH_2), HREI-MS: *m/z* calcd for $C_{15}H_{12}FN_5O$ $[M]^+$ 297.1026; Found; 297.1011.

3.2.4. 2-(1H-benzo[d][1,2,3]triazol-1-yl)-N′-(4-methylbenzylidene) acetohydrazide

^{1}H NMR (500 MHz, DMSOd_6) δ 11.59 (s, 1H, NH), 8.77 (s, 1H,

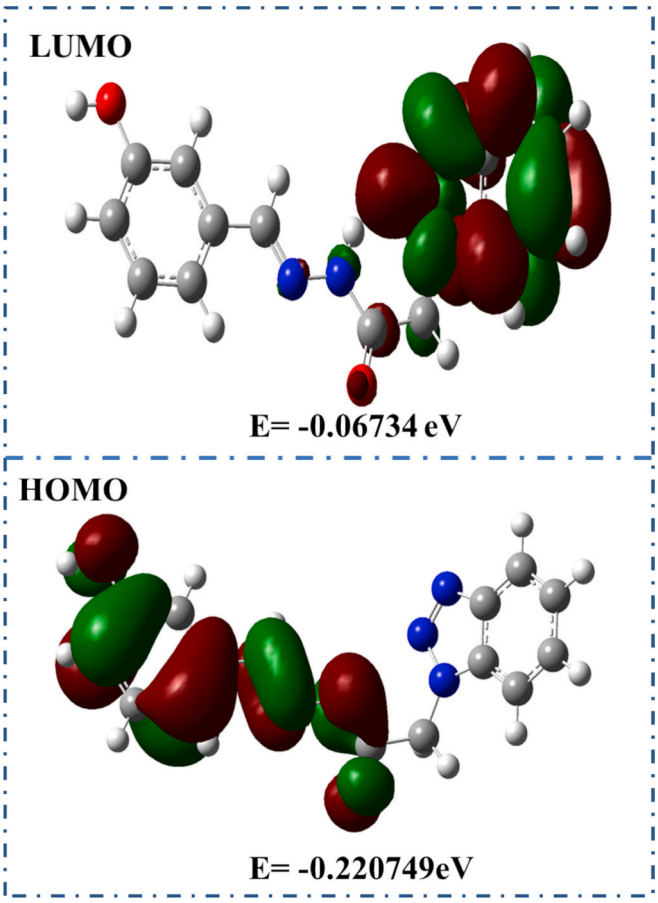

Fig. 9. FMO outcomes and HOMO-LUMO energy gap of analog 15.

N═CH), 7.98 (d, J = 8.2 Hz, 1H, ArH), 7.88 (d,d J = 1.85, 7.5 Hz, 2H, ArH), 7.38 (m, 2H, ArH), 7.32 (m, 2H, ArH), 7.09 (m, 1H, ArH), 4.32 (s, 2H, CH_2), 2.01 (s, 3H, CH_3), ^{13}C NMR (125 MHz, DMSOd_6) δ 167.2 (C), 141.3 (CH), 140.8 (C), 139.6 (C), 129.8 (C), 129.4 (C), 128.5 (CH), 128.5 (CH), 124.3 (CH), 124.3 (CH), 121.9 (CH), 121.3 (CH), 119.2 (CH), 109.4 (CH), 61.2 (CH_2), 21.3 (CH_3), HREI-MS: m/z calcd for $C_{16}H_{15}N_5O$ $[M]^{+}$ 293.1277; Found; 293.1262.

3.2.5. 2-(1H-benzo[d][1,2,3]triazol-1-yl)-N′-(3-methylbenzylidene) acetohydrazide

11.54 (s, 1H, NH), 8.43 (s, 1H, N═CH), 8.08 (d, J = 7.7 Hz, 1H, ArH), 7.81 (d, J = 7.5 Hz, 1H, ArH), 7.69 (s, 1H, ArH), 7.62 (d, J = 7.1 Hz, 1H, ArH), 7.56 (t, J = 7.6 Hz, 1H, ArH), 7.43 (t, J = 7.0 Hz, 1H, ArH), 7.29 (t, J = 7.6 Hz, 1H, ArH), 7.21 (d, J = 7.2 Hz, 1H, ArH), 5.33 (s, 2H, CH_2), 2.45 (s, 3H, CH_3), ^{13}C NMR (125 MHz, DMSOd_6) δ 167.7 (C), 142.4 (CH), 140.3 (C), 137.8 (C), 132.6 (C), 129.7 (CH), 129.0 (CH), 128.2 (CH), 127.2 (CH), 126.1 (C), 121.4 (CH), 121.2 (CH), 118.5 (CH), 109.3 (CH), 61.1 (CH_2), 21.2 (CH_3), HREI-MS: m/z calcd for $C_{16}H_{15}N_5O$ $[M]^{+}$ 293.1277; Found; 293.1262.

3.2.6. 2-(1H-benzo[d][1,2,3]triazol-1-yl)-N′-(2-methylbenzylidene) acetohydrazide

^{1}H NMR (500 MHz, DMSOd_6) δ 11.51 (s, 1H, NH), 8.29 (s, 1H, N═CH), 8.05 (d, J = 7.8 Hz, 1H, ArH), 7.65 (d, J = 7.2 Hz, 1H, ArH),7.81 (d, J = 7.4 Hz, 1H, ArH), 7.48 (t, J = 7.6 Hz, 1H, ArH), 7.24 (t, J = 7.7 Hz, 1H, ArH), 7.16 (d, J = 7.2 Hz, 1H, ArH), 7.11 (m, 2H, ArH), 5.22 (s, 2H, CH_2), 2.45 (s, 3H, CH_3), ^{13}C NMR (125 MHz, DMSOd_6) δ 166.5 (C), 140.9 (CH), 139.2 (C), 134.2 (C), 129.5 (C), 127.4 (C), 127.3 (CH), 126.8 (CH), 123.5 (CH), 123.0 (CH), 122.7 (CH), 121.5 (CH), 118.1 (CH), 107.6 (CH), 60.3 (CH_2), 18.9 (CH_3), HREI-MS: m/z calcd for $C_{16}H_{15}N_5O$ $[M]^{+}$ 293.1277; Found; 293.1262.

3.2.7. 2-(1H-benzo[d][1,2,3]triazol-1-yl)-N′-(2,4-dimethoxybenzylidene) acetohydrazide

^{1}H NMR (500 MHz, DMSOd_6) δ 11.71 (s, 1H, NH), 8.69 (s, 1H, N═CH), 8.14 (d, J = 7.8 Hz, 1H, ArH), 7.83 (d, J = 7.4 Hz, 1H, ArH), 7.57 (t, J = 7.5 Hz, 1H, ArH), 6.72 (s, 1H, ArH), 6.66 (d, J = 7.0 Hz, 1H, ArH), 7.32 (t, J = 7.5 Hz, 1H, ArH), 5.58 (s, 2H, CH_2), 3.84(s, 3H, OCH_3), 3.81 (s, 3H, OCH_3), ^{13}C NMR (125 MHz, DMSOd_6) δ 167.2 (C), 161.9 (C), 159.7 (C), 143.6 (CH), 142.1 (C), 132.2 (C), 131.3 (CH), 123.9 (CH), 123.2 (CH), 119.8 (CH), 110.8 (C), 109.6 (CH), 106.7 (CH), 103.1 (CH), 60.6 (CH_2), 55.7 (CH_3), 55.5 (CH_3), HREI-MS: m/z calcd for $C_{17}H_{17}N_5O_3$ $[M]^{+}$ 339.1331; Found; 339.1320.

3.2.8. 2-(1H-benzo[d][1,2,3]triazol-1-yl)-N′-(2-chlorobenzylidene) acetohydrazide

^{1}H NMR (500 MHz, DMSOd_6) δ 11.58 (s, 1H, NH), 8.65 (s, 1H, N═CH), 8.21 (d, J = 7.7 Hz, 1H, ArH), 8.03 (d, J = 7.6 Hz, 1H, ArH), 7.72 (d, J = 7.3 Hz, 1H, ArH), 7.63 (t, J = 7.4 Hz, 1H, ArH), 7.49 (m, 2H, ArH), 7.44 (d, J = 7.1 Hz, 1H, ArH),7.36 (t, J = 7.4 Hz, 1H, ArH), 5.51 (s, 2H, CH_2), ^{13}C NMR (125 MHz, DMSOd_6) δ 169.8 (C), 144.9, 138.2 (C), 136.3 (C), 134.6 (C), 133.4 (C), 133.1 (CH), 130.4 (CH), 127.2 (CH), 126.8 (CH), 125.7 (CH), 124.8 (CH), 122.9 (CH), 115.6 (CH), 61.9 (CH_2), HREI-MS: m/z calcd for $C_{15}H_{12}ClN_5O$ $[M]^{+}$ 313.0730; Found; 313.0713.

3.2.9. 2-(1H-benzo[d][1,2,3]triazol-1-yl)-N′-(4-chlorobenzylidene) acetohydrazide

^{1}H NMR (500 MHz, DMSOd_6) δ 11.66 (s, 1H, NH), 8.47 (s, 1H, N═CH), 8.25 (d, J = 7.8 Hz, 1H, ArH), 7.97 (d, J = 7.4 Hz, 1H, ArH), 76.88 (d, J = 7.2 Hz, 2H, ArH), 7.68 (t, J = 7.6 Hz, 1H, ArH), 7.46 (d, J = 6.9 Hz, 2H, ArH), 7.43 (t, J = 7.5 Hz, 1H, ArH), 5.55 (s, 2H, CH_2), ^{13}C NMR (125 MHz, DMSOd_6) δ 169.4 (C), 145.6 (CH), 142.6 (C), 137.3 (C), 134.8 (C), 132.3 (C), 131.9 (CH), 131.9 (CH), 130.4 (CH), 130.4 (CH), 125.0 (CH), 124.9 (CH), 122.4 (CH), 115.9 (CH), 62.4 (CH_2), HREI-MS: m/z calcd for $C_{15}H_{12}ClN_5O$ $[M]^{+}$ 313.0730; Found; 313.0713.

3.2.10. 2-(1H-benzo[d][1,2,3]triazol-1-yl)-N′-(2-nitrobenzylidene) acetohydrazide

^{1}H NMR (500 MHz, DMSOd_6) δ 12.57 (s, 1H, NH), 8.79 (s, 1H, N═CH), 8.56 (d, J = 6.5 Hz, 2H, ArH), 8.28 (d, J = 6.4 Hz, 1H, ArH), 7.93 (t, J = 6.6 Hz, 1H, ArH), 7.69 (t, J = 6.4 Hz, 2H, ArH), 7.56 (d, J = 6.7 Hz, 1H, ArH), 7.43 (t, J = 6.2 Hz, 1H, ArH), 5.08 (s, 2H, CH_2), ^{13}C NMR (125 MHz, DMSOd_6) δ 171.3 (C), 147.1 (C), 146.8 (CH), 146.4 (C), 135.5 (CH), 134.0 (C), 132.2 (CH), 130.6 (CH), 129.5 (C), 126.6 (CH), 126.1 (CH), 125.7 (CH), 124.9 (CH), 116.8 (CH), 63.2 (CH_2). HREI-MS: m/z calcd for $C_{15}H_{12}N_5O_3$ $[M]^{+}$ 324.0971; Found; 324.0958.

3.2.11. 2-(1H-benzo[d][1,2,3]triazol-1-yl)-N′-(3-nitrobenzylidene) acetohydrazide

^{1}H NMR (500 MHz, DMSOd_6) δ 11.82 (s, 1H, NH), 8.61 (s, 1H, N═CH), 8.55 (s, 1H, ArH), 8.32 (d, J = 7.9 Hz, 1H, ArH), 8.13 (d, J = 8.1 Hz, 1H, ArH), 8.09 (d, J = 8.1 Hz, 1H, ArH), 8.07 (d, J = 7.5 Hz, 1H, ArH), 7.77 (t, J = 7.7 Hz, 1H, ArH), 7.76 (m, 1H, ArH), 7.52 (t, J = 7.7 Hz, 1H, ArH), 5.67 (s, 2H, CH_2), ^{13}C NMR (125 MHz, DMSOd_6) δ 171.4 (C), 149.8 (C), 147.2 (CH), 145.8 (C), 135.8 (C), 132.5 (C), 133.9 (CH), 131.0 (CH), 128.8 (CH), 126.8 (CH), 126.2 (CH), 125.4 (CH), 124.3 (CH), 116.9 (CH), 63.5 (CH_2). HREI-MS: m/z calcd for $C_{15}H_{12}N_5O_3$ $[M]^{+}$ 324.0971; Found; 324.0958.

3.2.12. 2-(1H-benzo[d][1,2,3]triazol-1-yl)-N′-(4-nitrobenzylidene) acetohydrazide

^{1}H NMR (500 MHz, DMSOd_6) δ 11.79 (s, 1H, NH), 8.65 (s, 1H, N═CH), 8.36 (d, J = 8.2 Hz, 2H, ArH), 8.27 (d, J = 7.8 Hz, 1H, ArH), 8.02 (d, J = 7.4 Hz, 1H, ArH), 8.01 (d, J = 8.0 Hz, 2H, ArH),7.73 (t, J = 7.5 Hz, 1H, ArH), 7.43 (t, J = 7.5 Hz, 1H, ArH), 5.61 (s, 2H, CH_2), ^{13}C

NMR (125 MHz, DMSOd_6) δ 171.6 (C), 151.7 (C), 148.2 (CH), 147.4 (C), 140.0 (C), 134.2 (C), 127.2 (CH), 126.9 (CH), 126.8 (CH), 126.8 (CH_2), 126.3 (CH), 126.3 (CH), 125.3 (CH), 117.2 (CH), 63.9 (CH_2), HREI-MS: *m/z* calcd for $C_{15}H_{12}N_5O_3$ $[M]^{+}$ 324.0971; Found; 324.0958.

3.2.13. 2-(1H-benzo[d][1,2,3]triazol-1-yl)-N′-(4-hydroxybenzylidene) acetohydrazide

^{1}H NMR (500 MHz, DMSOd_6) δ 12.51 (s, 1H, NH), 11.06 (s, 1H, OH), 8.28 (s, 1H, N═CH), 8.10 (d, J = 7.3 Hz, 2H, ArH), 7.69 (m, 1H, ArH), 7.61 (d, J = 6.8 Hz, 1H, ArH), 7.55 (d, J = 6.7 Hz, 1H, ArH), 7.43 (t, J = 6.3 Hz, 1H, ArH), 7.12 (d, J = 7.3 Hz, 2H, ArH), 4.94 (s, 2H, CH_2), ^{13}C NMR (125 MHz, DMSOd_6) δ 169.6 (C), 161.4 (C), 145.9 (CH), 142.3 (C), 133.3 (C), 131.5 (CH), 131.5 (CH), 127.8 (C), 124.6 (CH), 124.4 (CH), 122.8 (CH), 118.1 (CH), 118.1 (CH), 114.4 (CH), 62.5 (CH_2), HREI-MS: *m/z* calcd for $C_{15}H_{13}N_5O_2$ $[M]^{+}$ 295.1069; Found; 295.1055.

3.2.14. 2-(1H-benzo[d][1,2,3]triazol-1-yl)-N′-(3,4-dimethoxybenzylidene)acetohydrazide

^{1}H NMR (500 MHz, DMSOd_6) δ 11.71 (s, 1H, NH), 8.49 (s, 1H, N═CH), 8.21 (d, J = 7.8 Hz, 1H, ArH), 7.89 (d, J = 7.6 Hz, 1H, ArH), 7.62 (s, 1H, ArH), 7.55 (t, J = 7.5 Hz, 1H, ArH), 7.41 (t, J = 7.6 Hz, 1H, ArH), 7.28 (d, J = 7.2 Hz, 1H, ArH), 7.04 (d, J = 7.1 Hz, 1H, ArH), 5.62 (s, 2H, CH_2), 3.85(s, 3H, OCH_3), 3.83 (s, 3H, OCH_3), ^{13}C NMR (125 MHz, DMSOd_6) δ 167.1 (C), 152.8 (C), 150.3 (C), 143.2 (CH), 141.6 (C), 131.4 (C), 130.8 (C), 123.4 (CH), 123.0 (CH), 122.5 (CH), 119.4 (CH), 113.7 (CH), 111.4 (CH), 109.5 (CH), 61.2 (CH2), 56.3 (CH3), 56.1 (CH3), HREI-MS: *m/z* calcd for $C_{17}H_{17}N_5O_3$ $[M]^{+}$ 339.1331; Found; 339.1320.

3.2.15. 2-(1H-benzo[d][1,2,3]triazol-1-yl)-N′-(3-hydroxybenzylidene) acetohydrazide

^{1}H NMR (500 MHz, DMSOd_6) δ 11.66 (s, 1H, NH), 8.45 (s, 1H, N═CH), 8.19 (d, J = 7.9 Hz, 1H, ArH), 7.95 (d, J = 7.6 Hz, 1H, ArH), 7.62 (t, J = 7.4 Hz, 1H, ArH), 7.33 (t, J = 7.5 Hz, 1H, ArH), 7.27 (m, 1H, ArH), 7.22 (s, 1H, ArH), 7.11 (m, 2H, ArH), 5.56 (s, 2H, CH_2), 9.77 (s, 1H, OH) ^{13}C NMR (125 MHz, DMSOd_6) δ 169.3 (C), 158.4 (C), 144.1 (CH), 142.2 (C), 138.8 (C), 133.7 (C), 130.5 (CH), 125.2 (CH), 124.1 (CH), 122.5 (CH), 121.2 (CH), 119.3 (CH), 115.7 (CH), 114.1 (CH), 61.8 (CH_2), HREI-MS: *m/z* calcd for $C_{15}H_{13}N_5O_2$ $[M]^{+}$ 295.1069; Found; 295.1055.

3.2.16. 2-(1H-benzo[d][1,2,3]triazol-1-yl)-N′-(2-hydroxybenzylidene) acetohydrazide

^{1}H NMR (500 MHz, DMSOd_6) δ 11.52 (s, 1H, NH), 8.67 (s, 1H, N═CH), 8.14 (d, J = 7.8 Hz, 1H, ArH), 7.91 (d, J = 7.6 Hz, 1H, ArH), 7.55 (t, J = 7.4 Hz, 1H, ArH), 7.52 (d, J = 7.0 Hz, 1H, ArH), 7.36 (m, 3H, ArH), 7.30 (t, J = 7.5 Hz, 1H, ArH), 5.47 (s, 2H, CH_2), 10.98 (s, 1H, OH), ^{13}C NMR (125 MHz, DMSOd_6) δ 168.5 (C), 156.8 (C), 143.2 (C), 142.9 (CH), 133.4 (C), 131.4 (CH), 126.4 (CH), 124.9 (CH), 124.3 (CH), 121.9 (CH), 121.1 (CH), 118.2 (C), 116.4 (CH), 113.7 (CH), 61.4 (CH_2), HREI-MS: *m/z* calcd for $C_{15}H_{13}N_5O_2$ $[M]^{+}$ 295.1069; Found; 295.1055.

3.2.17. 2-(1H-benzo[d][1,2,3]triazol-1-yl)-N′-(3-methoxybenzylidene) acetohydrazide

^{1}H NMR (500 MHz, DMSOd_6) δ 11.67 (s, 1H, NH), 8.55 (s, 1H, N═CH), 8.18 (d, J = 6.6 Hz, 1H, ArH), 7.90 (d, J = 6.6 Hz, 1H, ArH), 7.79 (d, J = 6.1 Hz, 1H, ArH), 7.54 (t, J = 3.0 Hz, 1H, ArH), 7.37 (s, 1H, ArH), 7.33 (t, J = 7.1 Hz, 1H, ArH), 7.24 (d, J = 6.5 Hz, 1H, ArH), 7.02 (d, J = 6.8 Hz, 1H, ArH), 5.22 (s, 2H, CH_2), 3.83 (s, 3H, OCH_3), ^{13}C NMR (125 MHz, DMSOd_6) δ 167.1 (C), 161.0 (C), 146.3 (CH), 141.1 (C), 139.7 (C), 132.2 (C), 130.3 (CH), 124.1 (CH), 123.6 (CH), 122.7 (CH), 119.4 (CH), 116.2 (CH), 113.5 (CH), 111.6 (CH), 61.7 (CH_2), 55.8 (CH_3), HREI-MS: m/z calcd for $C_{16}H_{15}N_5O_2$ $[M]^{+}$ 309.1226; Found; 309.1212.

3.2.18. 2-(1H-benzo[d][1,2,3]triazol-1-yl)-N′-(2-methoxybenzylidene) acetohydrazide

^{1}H NMR (500 MHz, DMSOd_6) δ 9.31 (s, 1H, NH), 8.52 (s, 1H, N═CH), 8.18 (d, J = 7.8 Hz, 1H, ArH), 7.92 (d, J = 7.4 Hz, 1H, ArH), 7.88 (d, J = 7.0 Hz, 1H, ArH), 7.63 (t, J = 7.5 Hz, 1H, ArH), 7.45 (t, J = 6.9 Hz, 1H, ArH), 7.39 (t, J = 7.5 Hz, 1H, ArH), 7.21 (t, J = 7.2 Hz, 1H, ArH), 7.09 (d, J = 6.8 Hz, 1H, ArH), 5.52 (s, 2H, CH_2), 3.83 (s, 3H, OCH_3), ^{13}C NMR (125 MHz, DMSOd_6) δ 166.9 (C), 157.7 (C), 146.1 (CH), 142.5 (C), 133.0 (C), 131.8 (CH), 131.3 (CH), 123.4 (CH), 123.0 (CH), 122.4 (CH), 120.2 (CH), 117.6 (C), 112.1 (CH), 110.7 (CH), 61.2 (CH_2), 55.3 (CH3), HREI-MS: m/z calcd for $C_{16}H_{15}N_5O_2$ $[M]^{+}$ 309.1226; Found; 309.1212.

3.3. Alpha-glucosidase inhibitory assay

The inhibition of α-glucosidase activity was assessed by the published procedure [48]. A solution of *Saccharomyces cerevisiae* dissolved in 100 mL of phosphate buffer (pH 6.8) and 200 mg of bovine serum albumin was used to obtain 1 mg of α-glucosidase. After that 10 μL of test compounds (1–100 μM) was mixed with 490 μL phosphate buffer (pH 6.8) and 250 μL of 5 mM *para*-nitrophenyl *α-D*-glucopyranoside. This mixture was incubated for 5 min at 37 °C, after incubation 250 μL α-glucosidase was added and further incubated for 15 min. Finally, 2000 μL Na_2CO_3 (200 mM) was added to reaction mixture. UV–Vis spectrophotometer was utilized to determine α-glucosidase activity at wavelength of 400 nm. The standard drug acarbose was used as positive control. The optimum concentration needed to hydrolyze 50 % of α-glucosidase was defined as the IC_{50} value. The percentage of inhibition was calculated using the following equation.

$$\%\text{Inhibition} = \frac{\text{A sample} - \text{A control}}{\text{A control}} \text{ x } 100$$

3.4. Docking protocol

To evaluate the inhibitory potential of synthetic compounds against alpha-glucosidase, a comprehensive molecular docking study was conducted using AutoDock. Initially, the crystallographic structure of α-(1, 4)-glucosidase is not available yet in the PDB, so we used homology modeling structural coordinated as suggested by Ming Liu et al. [49]. Initially the structure of the targeted protein was prepared by removing water molecules and any co-crystallized ligands that are not required for the study. For docking studies, the structures of the selected proteins were parameterized using AutoDock Tools [50]. In general, hydrogens were added to polar side chains to facilitate the formation of hydrogen bonds, and the Kollman and Gasteiger partial charges were calculated. AutoDock saved the prepared protein file in PDBQT format. The ligand, which is the synthetic compound of interest, is also prepared by generating its 3D structure, parameterized it, by adding hydrogen atoms, and compute Kollman and Gasteiger partial atomic charges. The ligand's rotatable bonds are defined to allow flexibility during the docking process, and it is saved in the PDBQT format. Docking simulations were performed with AutoDock using the Lamarkian genetic algorithm and default procedures to dock a flexible ligand to a rigid protein. The active site of alpha-glucosidase, where the ligands would be docked, was identified from the previous literature. Additionally, all the synthesized compounds were allowed to dock with the active site residues of the α-glucosidase. During the simulation, the software evaluates multiple conformations of the ligand by calculating the binding free energy for each pose, which allows it to predict the most favourable binding interactions. Once docking is complete, the resulting poses are ranked based on their binding energies (more negative score indicates higher affinity), and the best-scoring pose is selected for further analysis. The interactions between the ligand and receptor, such as hydrogen bonds and hydrophobic interactions, are examined to determine how the ligand fits into the binding pocket. Finally, the predicted protein–ligand interaction (PLI) was analyzed for molecular interactions using PyMol v 1.7 [51]. For docking validation, we performed a redocking procedure by docking the synthetic compounds again into the

enzyme's binding site [52]. The predicted binding poses were compared to ensure that the compounds docked in reasonable positions with good binding energies. To further confirm the accuracy of our docking results, we compared them with experimentally obtained active inhibitors against alpha-glucosidase, specifically focusing on the most active inhibitor based on IC_{50} values. The docking results showed similar trends, where the most active compounds had the best binding energies, while the least active compounds also showed weaker binding energies, consistent with experimental data. This consistency validates the reliability of our docking predictions.

4. Conclusion

New 1,2,3-benzotriazole-based Schiff base derivatives **(1–18)** were synthesized, characterized through different spectroscopic techniques and evaluated against alpha-glucosidase enzyme in the presence of standard drug acarbose. All the analogs exhibited good to excellent inhibitory potential. Among the series, the analog **13** having *para*-hydroxy substitution on phenyl ring with an IC_{50} value of 2.20 ± 0.30 μM was found to be the most potent inhibitor. Beside these eight other analogs **3, 8, 9, 10, 11, 12, 14,** and **16** were found to be more active than the standard drug acarbose. Structure-activity relationship (SAR) was established, which mainly depends upon the nature, number, and position of the substituents on the phenyl ring. Moreover, the binding interactions of highly potent scaffolds with the active site of both enzymes were elaborated through molecular docking. Compared to related published work, this study offers several distinct advantages. Firstly, our compounds exhibit improved inhibitory potency against alpha-glucosidase, with IC_{50} values significantly lower than those reported for similar scaffolds. Secondly, our SAR analysis provides a more detailed understanding of the substituent effects on inhibitory activity, enabling the rational design of more potent inhibitors. Finally, our molecular docking studies offer valuable insights into the binding interactions between our compounds and the active site of alpha-glucosidase, which can inform future optimization efforts. The potent compounds identified in this study hold promise for future therapeutic applications in diabetes treatment.

CRediT authorship contribution statement

Shawkat Hayat: Writing – original draft, Methodology. **Mohamed S. Othman:** Data curation. **Hayat Ullah:** Formal analysis, Conceptualization. **Amina Qureshi:** Writing – original draft. **Fazal Rahim:** Supervision, Project administration. **Sadiqa Begum:** Validation. **Mohsan Nawaz:** Investigation. **Abdul Wadood:** Software. **Amal H. Al-Bagawi:** Writing – review & editing, Visualization. **Ahmed M. Aref:** Writing – review & editing, Validation. **Mohamed A. Fareid:** Data curation. **Rashid Iqbal:** Visualization.

Funding

This research was funded by Scientific Research Deanship at University of Ha'il-Saudi Arabia through project number RG-23 161.

Declaration of competing interest

The authors declare that they have no known competing financial interests or personal relationships that could have appeared to influence the work reported in this paper.

Acknowledgments

This research was funded by Scientific Research Deanship at University of Ha'il-Saudi Arabia through project number RG-23 161.

Appendix A. Supplementary data

Supplementary data to this article can be found online at https://doi.org/10.1016/j.rechem.2025.102237.

Data availability

The data that has been used is confidential.

References

[1] H. Alrefai, H. Allababidi, S. Levy, J. Levy, The endocrine system in diabetes mellitus, Endocrine 18 (2002) 105–120.
[2] IDF (Ed.), International Diabetes Federation IDF Diabetes Atlas, 10th ed, IDF, Brussels, Belgium, 2021.
[3] J.H. Bae, K.D. Han, S.H. Ko, Y.S. Yang, K.C. Won, Diabetes fact sheet in Korea 2021, Diabetes Metab. J. 46 (2022) 417–426.
[4] F. Rahim, F. Malik, H. Ullah, A. Wadood, A. Rehman, K.M. Khan, Isatin based Schiff bases as inhibitors of α-glucosidase: synthesis, characterization, in vitro evaluation and molecular docking studies, Bioorg. Chem. 60 (2015) 42–48.
[5] B.K. Tripathi, A.K. Srivastava, Diabetes mellitus: complications and therapeutics RA130, Med. Sci. Monit. 12 (2006) 130–147.
[6] R. Hussain, M. Nabi, S. Khan, Z. Subhan, F. Rahim, M.S. Faisal, A. Hussain, H. Ullah, A.S. Algarni, S. Aghayeva, Design, synthesis and in vitro biological evaluation of new coumarin containing oxazole hybrid derivatives as multitarget inhibitor of α-amylase and α-glucosidase for the treatment of diabetes, Results Chem. 9 (2024) 101638.
[7] M. Li, L. Song, X. Qin, Advances in the cellular immunological pathogenesis of type 1 diabetes, J. Cell. Mol. Med. 18 (2014) 749–758.
[8] H. Ullah, I. Uddin, H.Z. Ali, W. Hassan, G. Mehnaz, L. Maryam, R. Iqbal, M. Nabi, A promising α-glucosidase and α-amylase inhibitors based on benzimidazole-oxadiazole hybrid analogues: evidence based in vitro and in silico studies, Results Chem. 11 (2024) 101832.
[9] W. Ullah, F. Rahim, S. Hayat, H. Ullah, M. Taha, S. Khan, A. Khaliq, K.M. Khan, Synthesis of indole based sulfonamide derivatives as potent inhibitors of α-glucosidase and α-amylase in management of type-II diabetes, Chem. Data Collections 50 (2024) 101122.
[10] A.D. Association, Standards of medical Care in Diabetes—2014. Diabetes Care 37, 2013, pp. S11–S66.
[11] S. Hayat, H. Ullah, F. Rahim, M. Sajid, A.N. Abdalla, Synthesis, biological evaluation and molecular docking study of benzimidazole derivatives as α-glucosidase inhibitors and anti-diabetes candidates, J. Mol. Struct. 1276 (2023) 134774.
[12] Y. Jiao, D. Hua, D. Huang, Q. Zhang, C. Yan, Characterization of a new heteropolysaccharide from green guava and its application as an α-glucosidase inhibitor for the treatment of type II diabetes, Food Funct. 9 (2018) 3997–4007.
[13] J.L. Chiasson, Acarbose for the prevention of diabetes, hypertension, and cardiovascular disease in subjects with impaired glucose tolerance: the study to prevent non-insulin-dependent diabetes mellitus (stop-Niddm) trial, Endocr. Pract. 12 (2006) 25–30.
[14] F. Rahim, K. Zaman, M. Taha, H. Ullah, F. Nawaz, K.M. Khan, Synthesis, in vitro alpha-glucosidase inhibitory potential of benzimidazole bearing bis-Schiff bases and their molecular docking study, Bioorg. Chem. 94 (2020) 103394.
[15] A.Y.A. Alzahrani, H. Ullah, F. Rahim, N. Iqbal, F. Nawaz, Synthesis, biological evaluation and in silico molecular modelling studies of Chloro substituted Bis-indole containing Benzohydrazide analogues as potential anti-diabetic and anti-Alzheimer's agents, J. Mol. Struct. 1316 (2024) 138908.
[16] F. Rahim, R. Hussain, S. Subhan, H. Ullah, M.M. Bekhit, M.S. Alnbaheen, A. S. Algarni, S. Aghayeva, Synthesis, in vitro β-glucuronidase inhibition of benzoxazole bearing thiosemicarbazide derivatives along with in silico molecular docking study, Results Chem. 9 (2024) 101635.
[17] M.S. Nadeem, S. Hayat, F. Rahim, J.A. Khan, H. Ullah, S. Iftikhar, K. Muhammad, Synthesis, biological evaluation, molecular docking and dynamic simulation of novel benzofuran derivatives as potential agents against Alzheimer's disease, J. Mol. Struct. 1322 (2025) 140279.
[18] V.S. Anjana, P.M. Kumar, An overview on medicinal perspective and biological behavior of benzotriazole; synthetic study on its multifaceted biological activities, 2025.
[19] S.D. Khalaf, N.A.A.S. Ahmed, A.H. Dalaf, Synthesis, characterization and biological evaluation (antifungal and antibacterial) of new derivatives of indole, benzotriazole and thioacetyl chloride, Mater. Today: Proceedings 47 (2021) 6201–6210.
[20] T.A. Jimoh, A.O. Oyewale, H. Ibrahim, J.D. Habila, D.E. Arthur, Biological evaluation and docking study of synthesized derivatives of benzotriazole and benzimidazole as antibacterial agents. Chemistry, Africa 5 (3) (2022) 509–523.
[21] A.N. Khayyat, K.O. Mohamed, A.M. Malebari, A. El-Malah, Design, synthesis, and anti-poliferative activities of novel substituted imidazole-thione linked benzotriazole derivatives, Molecules 26 (19) (2021) 5983.
[22] Q. Li, G. Liu, N. Wang, H. Yin, Z. Li, Synthesis and anticancer activity of benzotriazole derivatives, J. Heterocyclic Chem. 57 (3) (2020) 1220–1227.
[23] X. Wang, J. Du, T. Zhou, X. Fang, H. Yang, Novel benzotriazole-benzimidazole metal complexes: structure-activity relationship, synthesis, characterization, and antidiabetic activity, J. Mol. Struct. 1292 (2023) 136141.

[24] R. Ibba, S. Piras, P. Corona, F. Riu, R. Loddo, I. Delogu, G. Collu, G. Sanna, P. Caria, T. Dettori, A. Carta, Front. Chem. 9 (2021) 660424.
[25] G. Semple, P.J. Skinner, M.C. Cherrier, P.J. Webb, C.R. Sage, S.Y. Tamura, R. Chen, J.G. Richman, D.T. Connolly, J. Med. Chem. 49 (2006) 1227.
[26] H. Ullah, S. Ahmad, F. Khan, M. Taha, F. Rahim, A. Wadood, Synthesis, in-vitro and in-silico studies of triazinoindole bearing bis-Schiff base as β-glucuronidase inhibitors, J. Mol. Struct. 1244 (2021) 131003.
[27] H. Ullah, F. Rahim, M. Taha, K.M. Khan, Aryl-oxadiazole Schiff bases: synthesis, α-glucosidase in vitro inhibitory activity and their in-silico studies, Arab. J. Chem. 13 (2020) 4904–4915.
[28] J. Ceramella, D. Iacopetta, A. Catalano, F. Cirillo, M.S. Sinicropi, A review on the antimicrobial activity of Schiff bases: data collection and recent studies, Antibiotics 11 (2) (2022) 191.
[29] S. Kaya, S. Erkan, D. Karakaş, Computational investigation of molecular structures, spectroscopic properties and antitumor-antibacterial activities of some Schiff bases, Spectrochim. Acta A Mol. Biomol. Spectrosc. 244 (2021) 118829.
[30] N. Uddin, F. Rashid, S. Ali, S.A. Tirmizi, I. Ahmad, S. Zaib, A. Haider, Synthesis, characterization, and anticancer activity of Schiff bases, J. Biomol. Struct. Dyn. 38 (11) (2020) 3246–3259.
[31] K.M. Khan, H. Rasheed, B. Fatima, M. Hayat, F. Rahim, H. Ullah, S. Perveen, Anti-Cancer potential of benzophenone-Bis-Schiff bases on human pancreatic Cancer cell line, J. Chem. Soc. Pak. 38 (2016) 954–958.
[32] F. Rahim, M. Taha, H. Ullah, N. Uddin, M. Gollapalli, Synthesis of new arylhydrazide bearing Schiff bases/thiazolidinone: α-amylase, urease activities and their molecular docking studies, Bioorg. Chem. 91 (2019) 103112.
[33] S.E. Bhandarkar, P.P. Pathare, B.P. Khobragade, New nickel (II), copper (II) and cobalt (II) complexes based Salicyaldehyde Schiff Base: synthesis, characterisation, and antiviral activity, Mater. Today: Proceedings 92 (2023) 807–816.
[34] F. Rahim, H. Ullah, M. Taha, M.N. Khan, K.M. Khan, Synthesis and in vitro acetylcholinesterase and Butyrylcholinesterase inhibitory potential of hydrazide based Schiff bases, Bioorg. Chem. 68 (2016) 30–40.
[35] S. Arif, S. Khan, T. Iqbal, B.C. Yallur, F. Rahim, R. Hussain, Y. Khan, H. Ullah, Synthesis, characterization, DFT, AMDET and molecular docking reveals the binding mechanism of hydroxyl containing bis-Schiff base derivatives: an approach toward Alzheimer disease, Results Chem. 10 (2024) 101706.
[36] M. Mioc, C. Soica, V. Bercean, S. Avram, M. Balan-Porcarasu, D.A. Spandidos, Design, synthesis and pharmacotoxicological assessment of 5-mercapto-1, 2, 4-triazole derivatives with antibacterial and antiproliferative activity, Int. J. Oncol. 50 (2017) 1175–1183.
[37] S. Khan, H. Ullah, M. Taha, F. Rahim, M. Sarfraz, R. Iqbal, N. Iqbal, R. Hussain, S.A. A. Shah, K. Ayub, M.A. Albalawi, M.A. Abdelaziz, F.S. Alatawi, K.M. Khan, Synthesis, DFT studies, molecular docking and biological activity evaluation of Thiazole-sulfonamide derivatives as potent anti-Alzheimer's inhibitors, Molecules 28 (2023) 559.
[38] Z. Amjid, S. Khan, T. Iqbal, R. Hussain, H.Z. Ali, K. Shoaib, Y. Khan, H. Ullah, S. Arshad, R. Iqbal, R. Ullah, E.A. Ali, Synthesis, confirmations and biological evaluation of acid substituted Schiff base derivatives: unraveling insight through SAR, DFT, ADMET and molecular docking, Results Chem. 11 (2024) 101744.
[39] S. Khan, T. Iqbal, M. Rehman, R. Hussain, Y. Khan, H. Ullah, M. Ali, A. Hussain, S. Alfarraj, S.A. Alharbi, In vitro and in silico analysis for elucidation of α-amylase and α-glucosidase: synthesis, structural confirmation and drug likeness of benzothiazole derived thiazole base bis-Schiff base derivatives, Results Chem. 8 (2024) 101594.
[40] M. Frisch, F. Clemente, *Gaussian 09, Revision a. 01*; M.J. Frisch, G.W. Trucks, H.B. Schlegel, G.E. Scuseria, M.A. Robb, J.R. Cheeseman, G. Scalmani, V. Barone, B.G.A. Mennucci, Eds, Petersson, Gaussian, Inc., Wallingford, CT, USA, 2009.
[41] A.U. Khan, S. Muhammad, R.A. Khera, R.A. Shehzad, K. Ayub, J. Iqbal, DFT study of superhalogen (AlF4) doped boron nitride for tuning their nonlinear optical properties, Optik 231 (2021) 166464.
[42] M.D. Esrafili, N. Saeidi, DFT calculations on the catalytic oxidation of CO over Si-doped (6,0) boron nitride nanotubes, Struct. Chem. 27 (2015) 595–604.
[43] S. Khan, M. Yar, N. Kosar, K. Ayub, M. Arshad, M.N. Zahid, T. Mahmood, First-principles study for exploring the adsorption behavior of G-series nerve agents on graphdyine surface, Comput. Theor. Chem. 1191 (2020) 113043.
[44] O. Prasad, L. Sinha, N. Kumar, Theoretical Raman and IR spectra of tegafur and comparison of molecular electrostatic potential surfaces, polarizability and hyerpolarizability of tegafur with 5-fluoro-uracil by density functional theory, J. At. Mol. Sci. 1 (2010) 201–214.
[45] M. Hagar, H.A. Ahmed, G. Aljohani, O.A. Alhaddad, Investigation of some antiviral N-heterocycles as COVID 19 drug: molecular docking and DFT calculations, Int. J. Mol. Sci. 21 (2020) 3922.
[46] H.B. Liu, W.W. Gao, V.K.R. Tangadanchu, C.H. Zhou, R.X. Geng, Novel aminopyrimidinyl benzimidazoles as potentially antimicrobial agents: design, synthesis and biological evaluation, Eur. J. Med. Chem. 143 (2018) 66–84.
[47] E.S. Marinho, M.M. Marinho, A DFT study of synthetic drug topiroxostat: MEP, HOMO, LUMO, Int. J. Sci. Eng. Res. 7 (2016) 1264–1270.
[48] F. Rahim, H. Ullah, S.J. Gilani, M.N.B. Jumah, Thiadiazole based triazole/hydrazone derivatives: synthesis, in vitro α-glucosidase inhibitory activity and in silico molecular docking study, J. Mol. Struct. 1287 (2023) 135619.
[49] M. Liu, Synthesis and α-glucosidase inhibitory mechanisms of bis (2, 3-dibromo-4, 5-dihydroxybenzyl) ether, a potential marine bromophenol α-glucosidase inhibitor, Mar. Drugs 9 (9) (2011) 1554–1565.
[50] G.M. Morris, R. Huey, W. Lindstrom, M.F. Sanner, R.K. Belew, D.S. Goodsell, A. J. Olson, AutoDock4 and AutoDockTools4: automated docking with selective receptor flexibility, J. Comput. Chem. 30 (16) (2009) 2785–2791.
[51] W.L. DeLano, Pymol: an open-source molecular graphics tool, CCP4 Newsl. Protein Crystallogr 40 (1) (2002) 82–92.
[52] E. Mateev, I. Valkova, B. Angelov, M. Georgieva, A. Zlatkov, Validation through re-docking, cross-docking and ligand enrichment in various well-resoluted MAO-B receptors, Int. J. Pharm. Sci. Res. 13 (2022) 1000–1007.